



NIH Public Access

Author Manuscript

Biochemistry. Author manuscript; available in PMC 2012 July 26.

Published in final edited form as:

Biochemistry. 2011 July 26; 50(29): 6478–6487. doi:10.1021/bi200666h.

Friedreich's ataxia variants I154F and W155R diminish frataxin-based activation of the iron-sulfur cluster assembly complex[†]

Chi-Lin Tsai[®], Jennifer Bridwell-Rabb[®], and David P. Barondeau*

Abstract

Friedreich's ataxia (FRDA) is a progressive neurodegenerative disease that has been linked to defects in the protein frataxin (Fxn). Most FRDA patients have a GAA expansion in the first intron of their Fxn gene that decreases protein expression. Some FRDA patients have a GAA expansion on one allele and a missense mutation on the other allele. Few functional details are known for the ~15 different missense mutations identified in FRDA patients. Here *in vitro* evidence is presented that indicates the FRDA I154F and W155R variants bind more weakly to the complex of Nfs1, Isd11, and Isu2 and thereby are defective in forming the four-component SDUF complex that constitutes the core of the Fe-S cluster assembly machine. The binding affinities follow the trend Fxn ~ I154F > W155F > W155A ~ W155R. The Fxn variants also have diminished ability to function as part of the SDUF complex to stimulate the cysteine desulfurase reaction and facilitate Fe-S cluster assembly. Four crystal structures, including the first for a FRDA variant, reveal specific rearrangements associated with the loss of function and lead to a model for Fxn-based activation of the Fe-S cluster assembly complex. Importantly, the weaker binding and lower activity for FRDA variants correlate with the severity of disease progression. Together, these results suggest Fxn triggers sulfur transfer from Nfs1 to Isu2, and that these *in vitro* assays are sensitive and appropriate for deciphering functional defects and mechanistic details for human Fe-S cluster biosynthesis.

Keywords

crystal; structure/Fe-S; cluster; biosynthesis/frataxin/Friedreich's; ataxia/kinetics

Friedreich's ataxia (FRDA) is an autosomal recessive neurodegenerative disease caused by reduced amounts of the protein frataxin (Fxn) (1). The loss of Fxn results in a complex phenotype that includes increased iron in the mitochondria, deficiencies in Fe-S cluster enzymes, and enhanced sensitivity to oxidative stress (2). FRDA patients typically present symptoms during adolescence such as progressive limb and gait ataxia and often die prematurely from cardiomyopathy. There is currently no cure. The majority (>95%) of FRDA patients are homozygous for an unstable GAA trinucleotide repeat expansion in the first intron of the *FXN* gene (3). The number of repeats range from 7 to 40 for normal individuals and from 66 to >1700 for FRDA patients (3, 4). Importantly, larger numbers of GAA repeats correlate with lower Fxn expression and an earlier age of disease onset (5, 6). A small fraction of FRDA patients are compound heterozygotes with an expanded GAA repeat affecting one allele and a missense or nonsense mutation affecting the other allele (7).

[†]This work was supported in part by Texas A&M University, grant A-1647 from the Robert A. Welch foundation and grant 11BGIA5710009 from the American Heart Association.

*To whom correspondence should be addressed: Department of Chemistry, Texas A&M University, College Station, TX 77842, USA. Telephone: 979-458-0735. Fax: 979-458-0736. barondeau@tamu.edu.

[®]These authors contributed equally to this work.

For compound heterozygote patients, the Fxn protein levels do not necessarily correspond to the age of onset (3, 8).

Most researchers agree that Fxn has a critical role in iron-sulfur (Fe-S) cluster assembly (9, 10). Eukaryotic Fe-S cluster biosynthesis occurs in the matrix space of the mitochondria and involves at least a dozen proteins (11). $[2\text{Fe}-2\text{S}]^{2+/1+}$ clusters and, possibly, $[4\text{Fe}-4\text{S}]^{2+/1+}$ clusters are assembled on the monomeric Isu2 scaffold (12). Nfs1, which forms a functional complex with Isd11 (13–15), catalyzes the PLP-dependent breakdown of cysteine to alanine and produces a transient persulfide species on a mobile loop (16, 17). The sulfur from this persulfide species is then transferred to Isu2 and becomes the inorganic sulfide of the Fe-S clusters. After iron incorporation and Fe-S cluster synthesis, chaperones interact with the scaffold protein and assist in delivering intact Fe-S clusters to their apo targets (18–20). Many potential roles for Fxn in this process have been suggested, which is complicated by the presence of multiple Fxn proteolytic products (21–27). The 14 kDa monomeric form (referred to as Fxn in this manuscript) includes residues 81–210 and is commonly thought to function as an iron chaperone in Fe-S cluster biosynthesis (28). Both *in vivo* and *in vitro* data support pairwise physical interactions between eukaryotic Nfs1, Isd11, Isu1/2, and Fxn (13, 14, 29–33). Recently, biochemical evidence was provided for Nfs₁, Isd₁₁, and Isu₂ (SDU) and Nfs₁, Isd₁₁, Isu₂, and Fxn (SDUF) Fe-S cluster assembly complexes (34, 35). This work also identified Fxn as an allosteric activator of Fe-S cluster assembly that increases the catalytic efficiency (k_{cat}/K_M) for the cysteine desulfurase component of SDUF and the rate of Fe-S cluster biosynthesis (34).

The *FXN* missense mutations present in compound heterozygous patients likely cause at least partial defects in Fxn function that may provide additional insight into the role of Fxn in Fe-S cluster biosynthesis. Therefore, the human FRDA mutations I154F and W155R and related Fxn variants were investigated using our recently developed biochemical assays, combined with determination of X-ray crystal structures. The data indicated that these mutations and variants have defects in binding and activating the SDU complex. The relative effects of the I154F and W155R mutations *in vitro* correlate with the reported age of onset in patients. In addition, structure-function properties for the W155A, W155R and W155F variants contribute to a model for how Fxn triggers direct sulfur transfer from Nfs1 to Isu2 for Fe-S cluster assembly.

Experimental Procedures

Protein Preparation

The QuikChange method (Stratagene) was used to introduce point mutants (I154F, W155A, W155Rand W155F) into a pET11a plasmid containing human Fxn ($\Delta 1-55$) (34), and the mutation sites were confirmed by DNA sequencing. Plasmids containing the Fxn variants were individually transformed into *E. coli* strain BL21(DE3), and the cells were grown at 16 °C. Protein expression was induced at an OD_{600} of 0.6 with 0.5 mM IPTG. Cells were harvested 16 hours later and the Fxn variants were purified as previously described for native Fxn (34). The Fxn variants spontaneously truncate to a form that includes residues 82–210, based on N-terminal sequencing. The protein expression and purification of native Fxn, Isu2, and the Nfs₁/Isd₁₁ (SD) complex were performed as previously described (34). Protein concentrations for I154F, W155A, W155Rand W155F were estimated by their absorbance at 280 nm using extinction coefficients of 26030, 21430, 20340, and 21430 $M^{-1}cm^{-1}$, respectively.

Cysteine Desulfurase Activity Measurements

Reaction mixtures (800 μ L) containing SD (0.5 μ M), Isu2 (1.5 μ M), PLP (10 μ M), DTT (2 mM), $\text{Fe}(\text{NH}_4)_2(\text{SO}_4)_2$ (5 μ M), Fxn variants (1.5 μ M), 50 mM Tris pH 8.0, and 250 mM NaCl were incubated in an anaerobic glovebox (10~14 °C) for 30 minutes (34, 36, 37). The cysteine desulfurase reactions were initiated by addition of 100 μ M L-cysteine at 37 °C.

Sulfide production was typically linear for the first 30 minutes and an incubation time of 10 minutes was chosen to generate sufficient product for detection. Assays were quenched by addition of 100 μ L of 20 mM *N,N*-dimethyl-p-phenylenediamine in 7.2 N HCl and 100 μ L of 30 mM FeCl_3 in 1.2 N HCl, which also initiated the conversion of sulfide to methylene blue. After a twenty minute incubation at 37 °C, the absorption at 670 nm due to methylene blue formation was measured and compared with a Na_2S standard curve to quantitate sulfide production. Units are defined as $\mu\text{mol sulfide}/\mu\text{mol SD per minute at } 37^\circ\text{C}$. The rates for the cysteine desulfurase reaction were also examined in the presence of 10 equivalents of $\text{Fe}(\text{NH}_4)_2(\text{SO}_4)_2$ and with increasing amounts of Fxn to determine the number of equivalents, or the saturating amount, that are required to maximize the cysteine desulfurase activity. Batch one of Nfs1/Isd11 (cysteine desulfurase activity of 8.3 min^{-1}) was used for the initial Michaelis-Menten kinetics for all of the variants and the determination of the binding constants for the native Fxn, I154F and W155R variants. A second batch of SD with lower activity (4.8 min^{-1}) was used for determining the binding constants of the W155A and W155F Fxn variants.

An alternate cysteine desulfurase activity assay that monitored cysteine in solution (38) was used to verify the rate enhancement upon addition of Fxn variants. In this assay, reaction components were prepared at the same concentrations as the methylene blue assay (above), but at a final reaction volume of 50 μ L. After incubation in the anaerobic glovebox for 30 minutes, the cysteine desulfurase reaction was initiated with the addition of 100 μ M L-cysteine at 37 °C and quenched after 20 minutes using 50 μ L acetic acid. Next, 50 μ L of acid ninhydrin reagent 2 (stock solution was made by dissolving 25 mg ninhydrin in 600 μ L acetic acid and 400 μ L HCl) was added to the reaction mixtures, the sample were boiled for 10 minutes, rapidly cooled on ice, and diluted to 1 mL in 95% ethanol. The amount of cysteine reacted was quantitated using an extinction coefficient of $27.6 \text{ mM}^{-1}\text{cm}^{-1}$ at 560 nm (38) and compared to a sample that lacked enzyme.

Fe-S Cluster Formation on Isu2

Assay mixtures contained 8 μ M SD, 24 μ M Isu2, 24 μ M Fxn variants, 5 mM DTT, 200 μ M $\text{Fe}(\text{NH}_4)_2(\text{SO}_4)_2$, 100 μ M L-cysteine, 50 mM Tris pH 8.0, and 250 mM NaCl in a total volume of 0.2 mL. Isu2 was incubated with 5 mM DTT in 50 mM Tris pH 8, 250 mM NaCl in an anaerobic glovebox for 1 hour prior to mixing with the remaining assay components in an anaerobic cuvette. The reaction was initiated by injecting L-cysteine to a final concentration of 100 μ M with a gas-tight syringe. Fe-S cluster formation was monitored at 456 nm at room temperature and then the first 1000 seconds were fit as first-order kinetics using KaleidaGraph (Synergy Software). The rate was converted to the activity of Isu2 using an extinction coefficient of $9.8 \text{ mM}^{-1}\text{cm}^{-1}$ at 456 nm, previously determined for a presumed [2Fe-2S]²⁺ cluster bound to the human scaffold protein (39). Units are defined as the amount of Isu2 required to produce 1 μ mol of [2Fe-2S]²⁺ cluster / μ mol SDU complex per minute at 25 °C.

Michaelis-Menten Kinetics for Fxn Variants in SDUF Complex

The saturating amounts of the different Fxn variants were separately added to a standard reaction mixture (0.5 μ M SD, 1.5 μ M Isu2, 10 μ M PLP, 2 mM DTT, 5 μ M $\text{Fe}(\text{NH}_4)_2(\text{SO}_4)_2$, 50 mM Tris pH 8.0, and 250 mM NaCl) and incubated anaerobically for 30 minutes. The cysteine desulfurase activities were measured after initiating the reaction

with the substrate L-cysteine (0.01 to 1 mM). Reaction rates as a function of cysteine concentration were fit to the Michaelis-Menten equation using KaleidaGraph. The k_{cat} was also measured as a function of Fxn concentration and fit as a type II allosteric activator (40) to equation [1] using KaleidaGraph. In equation [1], K_d is the binding

$$k_{cat} = \frac{k_{SDU} + \frac{k_{SDUF}^{\infty} [Fxn]}{K_d}}{1 + \frac{[Fxn]}{K_d}} \quad [1]$$

constant, k_{SDU} is the k_{cat} in the absence of Fxn, and k_{SDUF}^{∞} is the k_{cat} with saturated amounts of Fxn.

Protein Crystallization, Data Collection, and Refinement

Protein crystallization trials were initiated with hanging-drop vapor diffusion methods by mixing 2 μ L of protein and 2 μ L of reservoir solution, followed by incubation at 22 °C. Native Fxn at 15 mg/mL in a 50 mM HEPES pH 7.5 buffer that included 50 mM NaCl was crystallized after a one month incubation with 30% 2-methyl-2,4-pentanediol, 0.1 M sodium citrate pH 5.6, and 0.2 M ammonium acetate. The crystals were flash frozen without additional cryoprotection. The W155R variant was concentrated to 25 mg/mL in a 25 mM HEPES pH 7.5 buffer and then crystallized after a three-day incubation with 16% PEG monomethyl ether 2000 and 0.1 M MES pH 6.0. Single crystals were transferred to a cryoprotection solution that included the reservoir solution plus 16% ethylene glycol for ~1 minute and flash frozen in liquid nitrogen. Initial crystallization conditions for the W155A variant at 10 mg/mL in a 50 mM Tris pH 7.5 buffer included 2.0 M ammonium sulfate, 0.2 M potassium sodium tartrate tetrahydrate, and 0.1 M sodium citrate tribasic dihydrate pH 5.0. These initial crystals were used for microseeding experiments using the same reservoir solution except the ammonium sulfate concentration was lowered to 1.8 M. Crystals of the W155F variant at 10 mg/mL in a 50 mM Tris pH 7.5 buffer were generated after incubation for a few months with a reservoir solution of 0.2 M sodium acetate trihydrate, 0.1 M Tris hydrochloride pH 8.5, and 30% PEG 4000. Single crystals of the W155A and W155F variants were transferred to a cryoprotection solution that included their respective reservoir solutions plus 20% glycerol for ~0.5 minutes and flash frozen in liquid nitrogen. X-ray diffraction data for native Fxn, W155Rand W155F crystals were collected at SSRL beamline 7-1 (ADSC Quantum-315R CCD detector), whereas diffraction data for the W155A variant was collected at APS beamline 23-ID-D (MAR 300 CCD detector). The images were integrated and scaled with iMosflm (41) and Scala of the CCP4 suite (42). Phases were determined by molecular replacement with Phaser (43), using a previously refined structure of human Fxn (44) as a search model (PDB code: 1EKG). Difference electron density and omit maps were manually fit with the XtalView package (45), and refined in Refmac5 (46) with all of the diffraction data, except for 5% used for R_{free} calculations (47). PDB codes are 3S4M for native Fxn, 3S5E for W155R3S5D for W155A, and 3S5F for W155F.

RESULTS

Diminished Allosteric Activation for Fxn Variants

Previously, human Fxn was shown to bind to the Nfs1, Isd11, Isu2 (SDU) complex and to stimulate sulfide production and Fe-S cluster biosynthesis (34). Here we tested the ability of purified recombinant I154F and W155R FRDA mutants as well as the related W155A and W155F variants to activate the SDU complex. These biochemical assays were performed using 3 equivalents of each Fxn variant, a cysteine concentration of 0.1 mM, which was chosen to mimic physiological conditions (48), and 10 equivalents of ferrous iron, which

further stimulates the rate of sulfide production for the SDUF complex (34). Each of the mutants exhibited a lower level of activation than native Fxn (Fxn > I154F > W155F > W155A > W155R), with the W155R mutation being most similar to a SDU sample that lacked Fxn (Fig. 1A and Table 1). A separate control assay monitored the depletion of cysteine and confirmed the Fxn-based activation and the diminished activity for the Fxn variants (Fig. 1B).

Diminished Fe-S Cluster Biosynthesis for Fxn Variants

Next, the rate of Fe-S cluster assembly on Isu2 was determined for each Fxn variant by monitoring increases in absorbance at 456 nm (39, 49). The SDUF complex with native Fxn exhibited an activity of $12.3 \mu\text{mol [2Fe-2S]} / \mu\text{mol SDU per minute}$ (Fig. 2), which is similar to the $6 \mu\text{mol [2Fe-2S]} / \mu\text{mol per minute}$ reported previously using the *Thermotoga maritima* NifS enzyme as the sulfur source and slightly different experimental conditions (39). All Fxn variants displayed lower Fe-S cluster assembly activities than native Fxn, with the W155R variant rate similar to a sample that lacked Fxn (Fig. 2 and Table 1). Control assays with $100 \mu\text{M}$ sulfide rather than cysteine exhibited significantly slower rates than any of the other samples indicating that efficient Fe-S formation was not mediated by sulfide in solution (Fig. 2). Overall, the relative activities for the different Fxn variants in the Fe-S cluster biosynthetic assay mirrored their ability to activate the cysteine desulfurase component of the assembly complex (Table 1).

Binding Constants for Fxn Variants

The activation defects of the Fxn variants could be due to defects in variant binding to SDU. We therefore determined binding constants for the Fxn variants by measuring the rates of sulfide production as a function of L-cysteine at different concentrations of added Fxn. The resulting k_{cat} values were plotted against the Fxn concentration and the data were fit as a type II allosteric activator to equation [1] (Fig. 3). A K_d of $0.22 \mu\text{M}$ was determined for native Fxn binding to SDU, which was similar to the $0.4 \mu\text{M}$ binding constant reported for the association of the Fxn homolog CyaY to the IscS/IscU complex (50); the prokaryotic IscS/IscU complex is analogous to the eukaryotic SDU complex. Each Fxn variant exhibited weaker binding to the SDU complex than native Fxn by a factor of 3 (I154F), 8 (W155F), 28 (W155A), and 30 (W155R) (Fig. 3 and Table 1).

Kinetic Parameters for Fxn Variants

The Michaelis-Menten kinetic parameters for the cysteine desulfurase reaction were determined for the SDUF complex with the different Fxn variants. To compensate for weaker binding of the different Fxn mutants, cysteine desulfurase activities were measured as a function of added Fxn. The cysteine desulfurase activity maximized, or saturated, after the addition of 3 equivalents of Fxn, 8 equivalents of I154F, 30 equivalents of W155F, 40 equivalents of W155A, and 40 equivalents of W155R (data not shown). Saturating amounts of the different Fxn variants were then added to the SDU complex and the rates of the cysteine desulfurase reaction were measured as a function of the L-cysteine concentration. The four Fxn variants exhibited lower k_{cat} values, but similar K_M values compared to native Fxn (Table 1). The most significant change was observed for the W155R variant, which lowered the k_{cat}/K_M by a factor of four.

Crystal Structures of Fxn Variants

High-resolution crystal structures were determined for native Fxn, plus the W155RW155A, and W155F variants to understand the structural basis for the altered functional properties (Table 2). The 1.30 \AA resolution native human Fxn structure contains N- and C-terminal α -helices that pack against an antiparallel β -sheet (Fig. 4A), as previously described (44, 51).

Overall, the structures of the W155A, W155Rand W155F variants displayed very similar backbone conformations with each exhibiting a $\text{C}\alpha$ RMSD of $< 0.5 \text{ \AA}$ compared to native Fxn. The primary structural differences were due to side-chain conformational changes near the mutation sites.

In the native human Fxn structure, electron density maps revealed that the W155 side chain is constrained by a hydrogen bond between the indole ring nitrogen and the side-chain oxygen of Q153 as well as van der Waals interactions with the side chains of R165 and Q148 (Fig. 4B). Q153 also forms a hydrogen bond to D167. The position of R165 is reinforced in the crystal structure by a hydrogen bond to residue E101 of a symmetry molecule in the $P_{2}12_12_1$ space group. Residue Q148 is the first residue in a class I- α RS α -turn (52) that connects β -strands 3 and 4, and its side-chain oxygen forms a hydrogen bond to the nitrogen of the N151 side-chain. Residues I154 and L156 are oriented in the opposite direction on β -strand 4 compared to W155, and make up part of the hydrophobic core of Fxn. Notably, there is a water-filled pocket on the Fxn surface near W155 that is on the opposite face of β -strand 4 from L156 (Figure 4B).

The W155A variant, which crystallized in the C2 space group, resulted in minor side chain rearrangements for residues N151 and R165 to form hydrogen bonds with Q153 (Fig. 4C). These new hydrogen bonds replaced the hydrogen bond to Q153 that was eliminated due to the loss of the indole ring. Residue Q153 maintained the native Fxn conformation and hydrogen bond to the D167 side-chain. A rearrangement of the N151 side-chain to interact with Q153 resulted in loss of the hydrogen bond between the N151 and Q148 side-chains observed in the native Fxn structure (Fig. 4D). Instead, the Q148 side-chain underwent a slight rearrangement to form a hydrogen bond to the backbone amide of residue 151 (Fig. 4C).

The FRDA mutation W155R crystallized in the $P_{2}12_12_1$ space group and exhibited a significant side-chain reorganization compared to native Fxn (Fig. 4D). A minor rearrangement for the side-chains of residues Q148 and N151 resulted in formation of hydrogen bonds with D115 of a symmetry molecule, whereas a conformational change for residue R165 resulted in formation of a salt bridge with E108 of a symmetry molecule (Fig. 4E). The FRDA mutant underwent a side-chain rotation for residue 155 to fill a cavity on the surface of Fxn (Fig. 4F) and formed hydrogen bonds to N146 and to E108 of a symmetry molecule. A $\sim 1.5 \text{ \AA}$ translation of the Q148- N151 α -turn between the third and fourth β -strand was also observed (Fig. 4D).

The W155F variant crystallized in the P_2_1 space group with two Fxn molecules in the asymmetric unit. The W155F structure revealed rearrangements to form a hydrogen bond between residues Q153 and N151 (Fig. 4G). The electron density for N151 indicated multiple side-chain conformations. A conformational change for residue R165 resulted in the formation of a hydrogen bond to the D139 carbonyl oxygen of an adjacent Fxn molecule (not shown). The W155F side-chain exhibited a rotated conformer compared to native Fxn and the phenylalanine filled the same cavity as the W155R side-chain (Fig. 4D and 4F). In addition, residue V144 underwent a rearrangement to better pack against the W155F side-chain. Together, these crystal structures showed minor rearrangements outside of the mutation site (Fig. 4D) and provided hints to the correlation between structural changes and the altered Fxn binding affinity and ability to function as an allosteric activator.

DISCUSSION

FXN missense mutations present in compound heterozygous patients were investigated to provide additional insight into the role of Fxn in Fe-S cluster biosynthesis, as these missense

mutations likely cause at least partial defects in Fxn function. Here the results showed that the FRDA missense mutations I154F and W155R and the related W155 variants W155A and W155F are impaired allosteric activators both for sulfide formation and for Fe-S cluster biosynthesis by the SDU complex. For the clinical mutations, W155R was much more defective *in vitro* than I154F. The clinical phenotype for patients with the I154F missense mutation and a GAA expansion are indistinguishable from individuals that are homozygous for the GAA repeat expansion (1, 6, 7). In contrast, individuals with the W155R missense mutation and a GAA expansion exhibit early onset FRDA pathogenesis (3, 53). Thus, the level of severity of the defects *in vitro* correlates with the clinical phenotypes.

In patients, several lines of evidence suggest that the I154F and W155R missense mutations could be compromised due to low *in vivo* protein levels similar to the effect of GAA repeat expansion (8, 54): the I154F and W155R mutants *in vitro* have decreased thermodynamic stability and a tendency to precipitate upon iron binding (51, 55, 56); the I154F mutation may (24) or may not (57) have slower *in vivo* maturation kinetics; and residues I154 and W155 are near K147, which is important for the ubiquitin-based degradation of Fxn (58).

Regardless of any defects in protein concentrations, previous *in vivo* data as well as *in vitro* data presented here suggest that the I154F and W155R additionally possess biochemical defects. The I154F mutation rescues the lethality of *FXN*^{-/-} mice, but also resulted in a FRDA-like phenotype that included loss of iron-sulfur cluster enzyme activity (59). The *Saccharomyces cerevisiae* *yfh1* alleles *W131A*, *W131F*, and *I130A* (equivalent to human *FXN* variants W155A, W155F, and I154A) also cause cellular growth defects on high-iron media and diminish aconitase activity similar to a deletion of *YFH1* that could be rescued by overexpression of *yfh1-W131F*, but not *yfh1-W131A* or *yfh1-I130A* (60). The Fxn variants tested here all had equivalent defects in the cysteine desulfurase (Fig. 1) and Fe-S cluster assembly (Fig. 2) assays relative to native Fxn, ranging from ~2-fold for I154F to ~14-fold for W155R (Table 1). As these *in vitro* assays cannot distinguish between mutants that do not bind the SDU complex from those that bind but cannot activate, the binding constants of the Fxn variants were determined (the I154F, W155F, W155A, and W155R variants bind 3-, 8-, 28-, and 30-fold weaker than native Fxn, respectively; Table 1). Weaker binding is consistent with previous pull down assays that reveal I154F and W155R Fxn variants have diminished binding to Isd11 (30), that the I154F mutant, but not the W155A or W155R variants, is capable of interacting with Nfs1 and IscU (35), and *S. cerevisiae* studies that indicate W131F, but not W131A, is able to interact with Isu1 (60). In addition, the recombinant Fxn variants exhibited 2- to 4-fold decreases in k_{cat}/K_M for cysteine turnover by the SDUF complex (Table 1). Weaker or non-productive binding by these mutants would exacerbate any effects of lower protein levels.

The Fxn binding constant and protein concentration in the mitochondria appear appropriately matched for a Fxn role in regulating Fe-S cluster biosynthesis. Although Fxn levels in human lymphocytes (61, 62), and buccal cells or whole blood (8) are known (in pg Fxn/μg total protein), the concentration of Fxn inside mitochondria from any human cell type, to the best of our knowledge, has not been reported. The concentration of Fxn has been estimated in yeast mitochondria to be 0.3 μM (63), based on global expression studies (64). Assuming this 0.3 μM frataxin concentration estimate is also accurate for human mitochondria, then the fraction of Fxn bound in the SDUF complex (equation [2]) with a K_d of 0.22 μM (Table 1) would be 58%. The concentration

$$\text{Fraction occupied} = \frac{[\text{SDUF}]}{[\text{SDU}] + [\text{SDUF}]} = \frac{[\text{Fxn}]}{[\text{Fxn}] + K_d} \times 100\% \quad [2]$$

of Fxn for FRDA patients was determined to be 4–29% (65), 29% (66), 21% (8), 27% (62), and 36% (54) of control Fxn levels. Lowering the Fxn level, for example, to ~25% of the normal Fxn concentration would decrease the activated SDUF fraction from 58% to 25%. Thus, the measured binding constant for native Fxn and the estimated level of Fxn in the mitochondria could explain the loss of Fe-S cluster activity for individuals with the GAA repeat expansion.

Interestingly, our results indicate that the cysteine desulfurase and Fe-S cluster activities appear to be correlated for the Fxn variants (Table 1). One explanation for this correlation is that the different Fxn variants affect the rate of persulfide cleavage from Nfs1 (Fig. 5A reaction A2) and the released sulfide combines with iron (in solution or on Isu2) to form Fe-S clusters (reaction A3). Two pieces of data argue against this model. First, substitution of 100 μM sulfide for the 100 μM cysteine in the Fe-S cluster [2] assembly assay resulted in no significant increase in absorbance in the time frame of the experiment (Fig. 2), inconsistent with reaction A3 (Fig. 5A). Second, the Fe-S assembly activities (determined at 25 °C) are faster than the cysteine desulfurase activities (measured at 37 °C) (Table 1). In scheme A, the rate of sulfide production reaction A2) is required to be as fast or faster than that for Fe-S cluster formation reaction A3). Together this data indicates the correlation for the cysteine desulfurase and Fe-S assembly activities is not due to differences in the ability of Fxn variants to facilitate DTT-induced release of sulfide from Nfs1.

An alternate explanation for this activity correlation is that Fxn induces rapid internal sulfur transfer from Nfs1 to Isu2. In this scheme (Fig. 5B), cysteine is converted to alanine by the SDU complex (reaction B1) and the resulting persulfide species on Nfs1 can be cleaved by DTT to produce sulfide (reaction B2). In the presence of Fxn, sulfur is transferred from the mobile loop on Nfs1 to generate a persulfide species on Isu2 (reaction B3). This persulfide species on Isu2 can then be reductively cleaved by DTT (reaction B4) or used for Fe-S cluster assembly (reaction B5). The Fxn-induced rate enhancement for the cysteine desulfurase reaction can be explained if Fxn induces rapid sulfur transfer from Nfs1 to Isu2 (reaction B3) and DTT cleavage of the persulfide on Isu2 (reaction B4) is faster than on Nfs1 (reaction B2). Moreover, the activity correlation for the Fxn variants could be explained by the common Fxn-induced sulfur transfer step (reaction B3) that depends on both Fxn binding and a Fxn-induced conformational change. In this model, the rate of Fe-S cluster formation (reaction B5) must be faster than sulfide release from Isu2 (reaction B4); otherwise the added DTT in the Fe-S cluster assay would cleave the persulfide prior to Fe-S cluster formation. Together the kinetic data suggest that Fxn affects the internal sulfur transfer (reaction B3) rather than the DTT-induced cleavage of a persulfide on Nfs1 (reaction A2). We therefore hypothesize that Fxn binding induces a conformational change that facilitates rapid sulfur transfer from Nfs1 to Isu2 for Fe-S cluster formation.

There is currently limited structural data for how Fxn interacts with the other components of the human Fe-S assembly complex. Here a comparison of native Fxn and W155A (Fig. 4B, 4C and 4D) variants revealed very minor structural differences, yet these variants have a 28-fold difference in binding affinity (Table 1). Tryptophan residues often participate in protein-protein interfaces through hydrophobic, π-π, and cation-π interactions (67, 68). W155 is stacked in a positively charged pocket on the surface of Fxn between R165 and Q148 (Fig. 4B and 4F). The W155A substitution diminishes a W155-dependent protrusion on the surface of Fxn (Fig. 4C) that could be part of the Fxn binding interface with the SDU complex. Alternately, W155 could undergo a conformational change, which would have minor steric clashes for an energetically favorable rotomer (Fig. 4F; orange), and fill a pocket on the surface of the protein that is on the opposite face of the β-sheet from L144 (Fig. 4B), which is occupied by the side-chain of residue 155 in the W155R (Fig. 4E) and W155F (Fig. 4G) structures. This induced-fit model (Fig. 6) might provide a protein partner

with opportunities for hydrophobic and π -stacking interactions with the indole ring of W155 that are not available in the native structure of Fxn. We hypothesize that the aromatic ring for W155 (and W155F) occupies this surface pocket on Fxn and interacts with a residue of SDU through π - π or cation- π interactions. In our working model, this interaction is important for both Fxn binding to the SDU complex and also in favoring a conformational change in Isu2 that positions a cysteine residue appropriately for sulfur transfer from Nfs1. The positively charged pocket between Fxn residues R165 and Q148 could form a separate interaction site in the Fe-S assembly complex. This scenario would explain the relative binding affinities of the W155 variants (Fxn > W155F > W155A, W155R), but requires evaluation through additional structure-function experiments. This hypothesis is also consistent with NMR studies of the Yfh1 homolog that suggests the Isu1 scaffold protein interacts primarily with residues of the N-terminal α -helix and the first three β -strands (69). Notably, the equivalent of Fxn W155R for the *E. coli* system, CyaY W61R also compromises protein function, despite the fact that CyaY is proposed to function as a suppressor rather than an activator of Fe-S cluster biosynthesis (70). Together these results highlight the importance of W155 in the SDU-Fxn interface and the differing roles Fxn-like regulators in the prokaryotes and eukaryotes that require further investigation.

In summary, we provide evidence that Fxn functions as a positive allosteric activator that may regulate human Fe-S cluster biosynthesis. The measured Fxn binding constant is similar to the estimated concentration of Fxn in mitochondria, which allows changes in Fxn levels to readily switch the Fe-S assembly complex on or off. The ~3–5 fold decrease in Fxn levels measured for FRDA patients would be expected to greatly decrease the amount of activated Fe-S assembly complex and explain the observed loss of activity for Fe-S containing enzymes *in vivo*. The FRDA W155R and I154F missense mutants exhibit decreased catalytic efficiency as allosteric activators and weaker binding to the Fe-S assembly complex that are consistent with the more severe pathogenesis of the W155R mutation. In our working model, Fxn undergoes a conformational change at residue W155 that triggers sulfur transfer from Nfs1 to Isu2 for Fe-S cluster assembly. Future studies are aimed at understanding the molecular basis for Fxn-induced sulfur transfer and providing additional mechanistic details for human Fe-S cluster biosynthesis.

Abbreviations

DTT	dithiothreitol
FRDA	Friedreich's ataxia
Fxn	frataxin
HEPES	N-2-hydroxyethylpiperazine-N'-2-ethanesulfonic acid
IPTG	isopropyl β -D-1-thiogalactopyranoside
MES	2-(N-morpholino)ethanesulfonic acid
PEG	polyethylene glycol
PLP	pyridoxal-5'-phosphate
S. cerevisiae	<i>Saccharomyces cerevisiae</i>
SD	Nfs1 Isd11 protein complex
SDU	Nfs1, Isd11, Isu2 protein complex
SDUF	Nfs1, Isd11, Isu2 and frataxin protein complex
Tris	Tris(hydroxymethyl)aminomethane

Acknowledgments

We thank Chris Putnam and James Vranish for helpful discussion and suggestions, Andrew Winn for making the W155F and W155A variants and assisting in crystal optimization, and Nick Fox for assistance in the ninhydrin experiments. Start-up funds from Texas A&M University are gratefully acknowledged. This project was supported in part by grant A-1647 from the Robert A. Welch foundation and grant 11BGIA5710009 from the American Heart Association. Portions of this research were carried out at the Stanford Synchrotron Radiation Laboratory, a national user facility operated by Stanford University on behalf of the U.S. Department of Energy, Office of Basic Energy Sciences. The SSRL Structural Molecular Biology Program is supported by the Department of Energy, Office of Biological and Environmental Research, and by the National Institutes of Health, National Center for Research Resources, Biomedical Technology Program, and the National Institute of General Medical Sciences. Use of the Advanced Photon Source was supported by the U. S. Department of Energy, Office of Science, Office of Basic Energy Sciences, under Contract No. DE-AC02-06CH11357.

References

1. Campuzano V, Montermini L, Moltè MD, Pianese L, Cossee M, Cavalcanti F, Monros E, Rodius F, Duclos F, Monticelli A, Zara F, Cañizares J, Koutnikova H, Bidichandani SI, Gellera C, Brice A, Trouillas P, De Michele G, Fillà A, De Frutos R, Palau F, Patel PI, Di Donato S, Mandel JL, Cocozza S, Koenig M, Pandolfo M. Friedreich's ataxia: autosomal recessive disease caused by an intronic GAA triplet repeat expansion. *Science*. 1996; 271:1423–1427. [PubMed: 8596916]
2. Schmucker S, Puccio H. Understanding the molecular mechanisms of Friedreich Ataxia to develop therapeutic approaches. *Hum Mol Genet*. 2010; 19:R103–R110. [PubMed: 20413654]
3. Santos R, Lefevre S, Sliwa D, Seguin A, Camadro J-M, Lesuisse E. Friedreich's Ataxia: Molecular Mechanisms, Redox Considerations and Therapeutic Opportunities. *Antioxid Redox Signal*. 2010; 13:651–690. [PubMed: 20156111]
4. Schöls L, Amoiridis G, Przuntek H, Frank G, Epplen JT, Epplen C. Friedreich's ataxia. Revision of the phenotype according to molecular genetics. *Brain*. 1997; 120(Pt 12):2131–2140. [PubMed: 9448568]
5. Dürr A, Cossee M, Agid Y, Campuzano V, Mignard C, Penet C, Mandel JL, Brice A, Koenig M. Clinical and genetic abnormalities in patients with Friedreich's ataxia. *N Engl J Med*. 1996; 335:1169–1175. [PubMed: 8815938]
6. Fillà A, De Michele G, Cavalcanti F, Pianese L, Monticelli A, Campanella G, Cocozza S. The relationship between trinucleotide (GAA) repeat length and clinical features in Friedreich ataxia. *Am J Hum Genet*. 1996; 59:554–560. [PubMed: 8751856]
7. Cossee M, Dürr A, Schmitt M, Dahl N, Trouillas P, Allinson P, Kostrzewa M, Nivelon-Chevallier A, Gustavson KH, Kohlschütter A, Müller U, Mandel JL, Brice A, Koenig M, Cavalcanti F, Tammaro A, De Michele G, Fillà A, Cocozza S, Labuda M, Montermini L, Poirier J, Pandolfo M. Friedreich's ataxia: point mutations and clinical presentation of compound heterozygotes. *Ann Neurol*. 1999; 45:200–206. [PubMed: 9989622]
8. Deutsch EC, Santani AB, Perlman SL, Farmer JM, Stolle CA, Marusich MF, Lynch DR. A rapid, noninvasive immunoassay for frataxin: Utility in assessment of Friedreich ataxia. *Mol Genet Metab*. 2010; 101:238–245. [PubMed: 20675166]
9. Muhlenhoff U, Richhardt N, Ristow M, Kispal G, Lill R. The yeast frataxin homolog Yfh1p plays a specific role in the maturation of cellular Fe/S proteins. *Hum Mol Genet*. 2002; 11:2025–2036. [PubMed: 12165564]
10. Stehling O, Elsässer H, Brückel B, Muhlenhoff U, Lill R. Iron-sulfur protein maturation in human cells: evidence for a function of frataxin. *Hum Mol Genet*. 2004; 13:3007–3015. [PubMed: 15509595]
11. Rouault TA, Tong W-H. Iron-sulfur cluster biogenesis and human disease. *Trends Genet*. 2008; 24:398–407. [PubMed: 18606475]
12. Foster MW, Mansy SS, Hwang J, Penner-Hahn JE, Sureris KK, Cowan JA. A Mutant Human IscU Protein Contains a Stable [2Fe2S]2+ Center of Possible Functional Significance. *J Am Chem Soc*. 2000; 122:6805–6806.

13. Adam AC, Bornhövd C, Prokisch H, Neupert W, Hell K. The Nfs1 interacting protein Isd11 has an essential role in Fe/S cluster biogenesis in mitochondria. *Embo J.* 2006; 25:174–183. [PubMed: 16341090]
14. Shi Y, Ghosh M, Tong W-H, Rouault TA. Human ISD11 is essential for both iron-sulfur cluster assembly and maintenance of normal cellular iron homeostasis. *Hum Mol Genet.* 2009; 18:3014–3025. [PubMed: 19454487]
15. Wiedemann N, Urzica E, Guiard B, Müller H, Lohaus C, Meyer HE, Ryan MT, Meisinger C, Muhlenhoff U, Lill R, Pfanner N. Essential role of Isd11 in mitochondrial iron-sulfur cluster synthesis on Isu scaffold proteins. *Embo J.* 2006; 25:184–195. [PubMed: 16341089]
16. Zheng L, White RH, Cash VL, Jack RF, Dean DR. Cysteine desulfurase activity indicates a role for NIFS in metallocluster biosynthesis. *Proc Natl Acad Sci USA.* 1993; 90:2754–2758. [PubMed: 8464885]
17. Lill R. Function and biogenesis of iron-sulphur proteins. *Nature.* 2009; 460:831–838. [PubMed: 19675643]
18. Hoff KG, Silberg JJ, Vickery L. Interaction of the iron-sulfur cluster assembly protein IscU with the Hsc66/Hsc20 molecular chaperone system of Escherichia coli. *Proc Natl Acad Sci USA.* 2000; 97:7790–7795. [PubMed: 10869428]
19. Uhrigshardt H, Singh A, Kovtunovich G, Ghosh M, Rouault TA. Characterization of the human HSC20, an unusual DnaJ type III protein, involved in iron-sulfur cluster biogenesis. *Hum Mol Genet.* 2010; 19:3816–3834. [PubMed: 20668094]
20. Füzéry A, Tonelli M, Ta D, Cornilescu G, Vickery L, Markley J. Solution Structure of the Iron-Sulfur Cluster Chaperone HscB and Its Binding Surface for the Iron-Sulfur Assembly Scaffold Protein IscU. *Biochemistry.* 2008; 47:9394–9404. [PubMed: 18702525]
21. Cavadini P, Adamec J, Taroni F, Gakh O, Isaya G. Two-step processing of human frataxin by mitochondrial processing peptidase. Precursor and intermediate forms are cleaved at different rates. *J Biol Chem.* 2000; 275:41469–41475. [PubMed: 11020385]
22. Schmucker S, Argentini M, Carelle-Calmels N, Martelli A, Puccio H. The in vivo mitochondrial two-step maturation of human frataxin. *Hum Mol Genet.* 2008; 17:3521–3531. [PubMed: 18725397]
23. Long S, Jirku M, Ayala FJ, Lukes J. Mitochondrial localization of human frataxin is necessary but processing is not for rescuing frataxin deficiency in Trypanosoma brucei. *Proc Natl Acad Sci USA.* 2008; 105:13468–13473. [PubMed: 18768799]
24. Koutnikova H, Campuzano V, Koenig M. Maturation of wild-type and mutated frataxin by the mitochondrial processing peptidase. *Hum Mol Genet.* 1998; 7:1485–1489. [PubMed: 9700204]
25. Branda SS, Cavadini P, Adamec J, Kalousek F, Taroni F, Isaya G. Yeast and human frataxin are processed to mature form in two sequential steps by the mitochondrial processing peptidase. *J Biol Chem.* 1999; 274:22763–22769. [PubMed: 10428860]
26. Condo I, Ventura N, Malisan F, Rufini A, Tomassini B, Testi R. In vivo maturation of human frataxin. *Hum Mol Genet.* 2007; 16:1534–1540. [PubMed: 17468497]
27. Yoon T, Dizin E, Cowan JA. N-terminal iron-mediated self-cleavage of human frataxin: regulation of iron binding and complex formation with target proteins. *J Biol Inorg Chem.* 2007; 12:535–542. [PubMed: 17285345]
28. Stemmler TL, Lesuisse E, Pain D, Dancis A. Frataxin and mitochondrial Fe-S cluster biogenesis. *J Biol Chem.* 2010; 285:26737–26743. [PubMed: 20522547]
29. Gerber J, Muhlenhoff U, Lill R. An interaction between frataxin and Isu1/Nfs1 that is crucial for Fe/S cluster synthesis on Isu1. *EMBO Rep.* 2003; 4:906–911. [PubMed: 12947415]
30. Shan Y, Napoli E, Cortopassi GA. Mitochondrial frataxin interacts with ISD11 of the NFS1/ISCU complex and multiple mitochondrial chaperones. *Hum Mol Genet.* 2007; 16:929–941. [PubMed: 17331979]
31. Ramazzotti A, Vanmansart V, Foury F. Mitochondrial functional interactions between frataxin and Isu1p, the iron-sulfur cluster scaffold protein, in *Saccharomyces cerevisiae*. *FEBS Lett.* 2004; 557:215–220. [PubMed: 14741370]

32. Yoon T, Cowan J. Iron-sulfur cluster biosynthesis. Characterization of frataxin as an iron donor for assembly of [2Fe-2S] clusters in ISU-type proteins. *J Am Chem Soc.* 2003; 125:6078–6084. [PubMed: 12785837]
33. Wang T, Craig EA. Binding of yeast frataxin to the scaffold for Fe-S cluster biogenesis, Isu. *J Biol Chem.* 2008; 283:12674–12679. [PubMed: 18319250]
34. Tsai C-L, Barondeau DP. Human frataxin is an allosteric switch that activates the Fe-S cluster biosynthetic complex. *Biochemistry.* 2010; 49:9132–9139. [PubMed: 20873749]
35. Schmucker S, Martelli A, Colin F, Page A, Wattenhofer-Donzé M, Reutener L, Puccio H. Mammalian Frataxin: An Essential Function for Cellular Viability through an Interaction with a Preformed ISCU/NFS1/ISD11 Iron-Sulfur Assembly Complex. *PLoS ONE.* 2011; 6:e16199. [PubMed: 21298097]
36. Marelja Z, Stöcklein W, Nimtz M, Leimkühler S. A novel role for human Nfs1 in the cytoplasm: Nfs1 acts as a sulfur donor for MOCS3, a protein involved in molybdenum cofactor biosynthesis. *J Biol Chem.* 2008; 283:25178–25185. [PubMed: 18650437]
37. Siegel LM. A direct microdetermination for sulfide. *Anal Biochem.* 1965; 11:126–132. [PubMed: 14328633]
38. Winn MD, Ballard CC, Cowtan KD, Dodson EJ, Emsley P, Evans PR, Keegan RM, Krissinel EB, Leslie AG, McCoy A, McNicholas SJ, Murshudov GN, Pannu NS, Potterton EA, Powell HR, Read RJ, Vagin A, Wilson KS. Overview of the CCP4 suite and current developments. *Acta Crystallogr D Biol Crystallogr.* 2011; 67:235–242. [PubMed: 21460441]
39. Huang J, Cowan JA. Iron-sulfur cluster biosynthesis: role of a semi-conserved histidine. *Chem Commun (Camb).* 2009; 21:3071–3073. [PubMed: 19462090]
40. Di Cera E. Kinetics of Allosteric Activation. *Methods in Enzymology, Vol 466: Biothermodynamics, Pt B.* 2009; 466:259–271.
41. Leslie AGW. Recent changes to the MOSFLM package for processing film and image plate data. *Joint CCP4 + ESF-EAMCB Newsletter on Protein Crystallography.* 1992
42. The CCP4 suite: programs for protein crystallography. *Acta Crystallogr D Biol Crystallogr.* 1994; 50:760–763. [PubMed: 15299374]
43. McCoy AJ, Grosse-Kunstleve RW, Adams PD, Winn MD, Storoni LC, Read RJ. Phaser crystallographic software. *J Appl Crystallogr.* 2007; 40:658–674. [PubMed: 19461840]
44. Dhe-Paganon S, Shigeta R, Chi YI, Ristow M, Shoelson SE. Crystal structure of human frataxin. *J Biol Chem.* 2000; 275:30753–30756. [PubMed: 10900192]
45. McRee DE. XtalView/Xfit A Versatile Program for Manipulating Atomic Coordinates and Electron Density. *Journal of Structural Biology.* 1999; 125:156–165. [PubMed: 10222271]
46. Winn MD, Murshudov GN, Papiz MZ. Macromolecular TLS refinement in REFMAC at moderate resolutions. *Methods Enzymol.* 2003; 374:300–321. [PubMed: 14696379]
47. Brunger AT. The Free R value: a Novel Statistical Quantity for Assessing the Accuracy of Crystal Structures. *Nature.* 1992; 355:472–474. [PubMed: 18481394]
48. Furne J, Saeed A, Levitt MD. Whole tissue hydrogen sulfide concentrations are orders of magnitude lower than presently accepted values. *Am J Physiol Regul Integr Comp Physiol.* 2008; 295:R1479–R1485. [PubMed: 18799635]
49. Agar J, Krebs C, Frazzon J, Huynh BH, Dean DR, Johnson M. IscU as a scaffold for iron-sulfur cluster biosynthesis: sequential assembly of [2Fe-2S] and [4Fe-4S] clusters in IscU. *Biochemistry.* 2000; 39:7856–7862. [PubMed: 10891064]
50. Prischi F, Konarev PV, Iannuzzi C, Pastore C, Adinolfi S, Martin SR, Svergun DI, Pastore A. Structural bases for the interaction of frataxin with the central components of iron-sulphur cluster assembly. *Nat Commun.* 2010; 1:95. [PubMed: 20981023]
51. Musco G, Stier G, Kolmerer B, Adinolfi S, Martin SR, Frenkel TA, Gibson TJ, Pastore A. Towards a structural understanding of Friedreich's ataxia: the solution structure of frataxin. *Structure.* 2000; 8:695–707. [PubMed: 10903947]
52. Pavone V, Gaeta G, Lombardi A, Nastri F, Maglio O, Isernia C, Saviano M. Discovering protein secondary structures: classification and description of isolated alpha-turns. *Biopolymers.* 1996; 38:705–721. [PubMed: 8652792]

53. Poirier J, Pandolfo M. A missense mutation (W155R) in an American patient with Friedreich Ataxia. *Hum Mutat.* 1999;
54. Saccà F, Puorro G, Antenora A, Marsili A, Denaro A, Piro R, Sorrentino P, Pane C, Tessa A, Brescia Morra V, Cocozza S, De Michele G, Santorelli FM, Filla A. A combined nucleic Acid and protein analysis in friedreich ataxia: implications for diagnosis, pathogenesis and clinical trial design. *PLoS ONE.* 2011; 6:e17627. [PubMed: 21412413]
55. Correia AR, Adinolfi S, Pastore A, Gomes CM. Conformational stability of human frataxin and effect of Friedreich's ataxia-related mutations on protein folding. *Biochem J.* 2006; 398:605–611. [PubMed: 16787388]
56. Correia A, Pastore C, Adinolfi S, Pastore A, Gomes C. Dynamics, stability and iron-binding activity of frataxin clinical mutants. *FEBS J.* 2008; 275:3680–3690. [PubMed: 18537827]
57. Gordon DM, Shi Q, Dancis A, Pain D. Maturation of frataxin within mammalian and yeast mitochondria: one-step processing by matrix processing peptidase. *Hum Mol Genet.* 1999; 8:2255–2262. [PubMed: 10545606]
58. Rufini A, Fortuni S, Arcuri G, Condo' I, Serio D, Incani O, Malisan F, Ventura N, Testi R. Preventing the ubiquitin/proteasome-dependent degradation of frataxin, the protein defective in Friedreich's Ataxia. *Hum Mol Genet.* 2011
59. Calmels N, Schmucker S, Wattenhofer-Donzé M, Martelli A, Vaucamps N, Reutenaer L, Messadeq N, Bouton C, Koenig M, Puccio H. The first cellular models based on frataxin missense mutations that reproduce spontaneously the defects associated with Friedreich ataxia. *PLoS ONE.* 2009; 4:e6379. [PubMed: 19629184]
60. Leidgens S, De Smet S, Foury F. Frataxin interacts with Isu1 through a conserved tryptophan in its beta-sheet. *Hum Mol Genet.* 2010; 19:276–286. [PubMed: 19884169]
61. Boehm T, Scheiber-Mojdehkar B, Kluge B, Goldenberg H, Laccone F, Sturm B. Variations of frataxin protein levels in normal individuals. *Neurol Sci.* 2011; 32:327–330. [PubMed: 20506029]
62. Steinkellner H, Scheiber-Mojdehkar B, Goldenberg H, Sturm B. A high throughput electrochemiluminescence assay for the quantification of frataxin protein levels. *Anal Chim Acta.* 2010; 659:129–132. [PubMed: 20103114]
63. Hudder B, Morales J, Stubna A, Müncck E, Hendrich M, Lindahl P. Electron paramagnetic resonance and Mössbauer spectroscopy of intact mitochondria from respiring *Saccharomyces cerevisiae*. *J Biol Inorg Chem.* 2007; 12:1029–1053. [PubMed: 17665226]
64. Ghaemmaghami S, Huh W-K, Bower K, Howson RW, Belle A, Dephoure N, O'Shea EK, Weissman JS. Global analysis of protein expression in yeast. *Nature.* 2003; 425:737–741. [PubMed: 14562106]
65. Campuzano V, Montermini L, Lutz Y, Cova L, Hindelang C, Jiralerspong S, Trottier Y, Kish SJ, Faucheu B, Trouillas P, Authier Fo, Dürr A, Mandel JL, Vescovi A, Pandolfo M, Koenig M. Frataxin is reduced in Friedreich ataxia patients and is associated with mitochondrial membranes. *Hum Mol Genet.* 1997; 6:1771–1780. [PubMed: 9302253]
66. Willis J, Isaya G, Gakh O, Capaldi R, Marusich M. Lateral-flow immunoassay for the frataxin protein in Friedreich's ataxia patients and carriers. *Mol Genet Metab.* 2008; 94:491–497. [PubMed: 18485778]
67. Ma B, Elkayam T, Wolfson H, Nussinov R. Protein-protein interactions: structurally conserved residues distinguish between binding sites and exposed protein surfaces. *Proc Natl Acad Sci U S A.* 2003; 100:5772–5777. [PubMed: 12730379]
68. Gallivan JP, Dougherty DA. Cation-pi interactions in structural biology. *Proc Natl Acad Sci USA.* 1999; 96:9459–9464. [PubMed: 10449714]
69. Cook JD, Kondapalli KC, Rawat S, Childs WC, Murugesan Y, Dancis A, Stemmler TL. Molecular details of the yeast frataxin-Isu1 interaction during mitochondrial Fe-S cluster assembly. *Biochemistry.* 2010; 49:8756–8765. [PubMed: 20815377]
70. Adinolfi S, Iannuzzi C, Prischi F, Pastore C, Iametti S, Martin S, Bonomi F, Pastore A. Bacterial frataxin CyaY is the gatekeeper of iron-sulfur cluster formation catalyzed by IscS. *Nat Struct Mol Biol.* 2009; 16:390–396. [PubMed: 19305405]

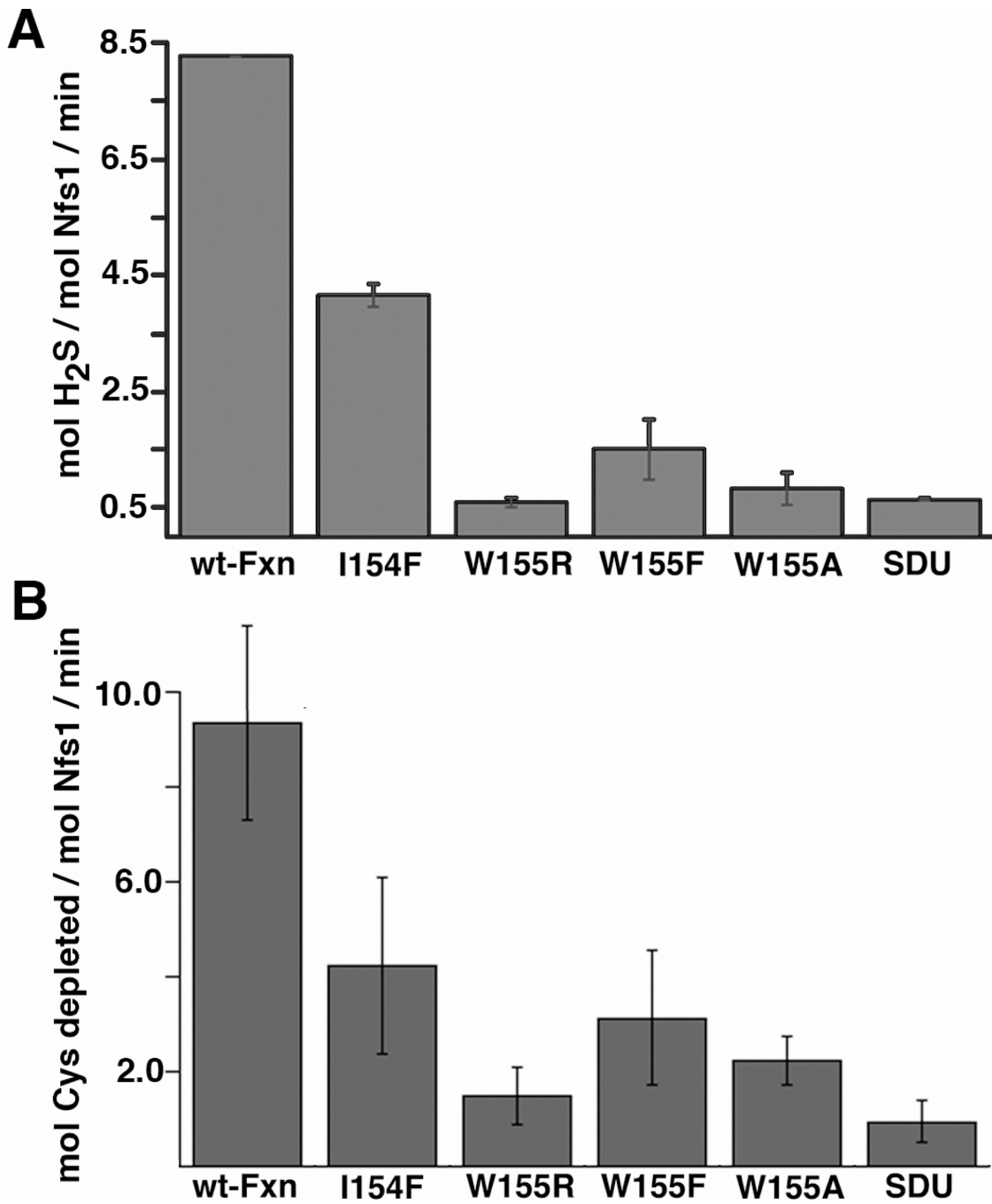


Figure 1.

Fxn variants show diminished ability to activate cysteine desulfurase activities for the Fe-S assembly complex. Cysteine desulfurase activity was determined spectrophotometrically in the presence of 1 equivalent of the Nfs1/Isd11 complex, 3 equiv of each Fxn variants, 3 equiv of Isu2, and 10 equiv. of ferrous iron. A) Activity was determined by converting generated sulfide to methylene blue. B) Activity was determined by reacting cysteine in solution with ninhydrin. Error bars are for at least three independent measurements.

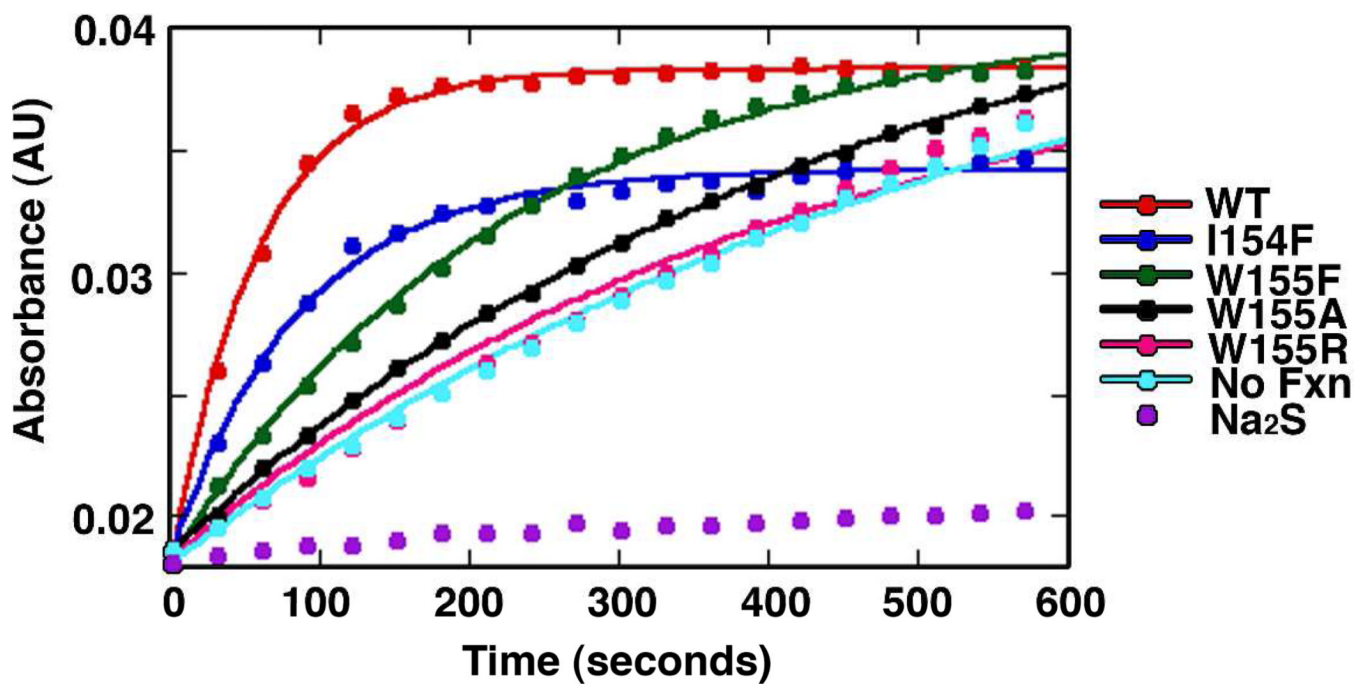
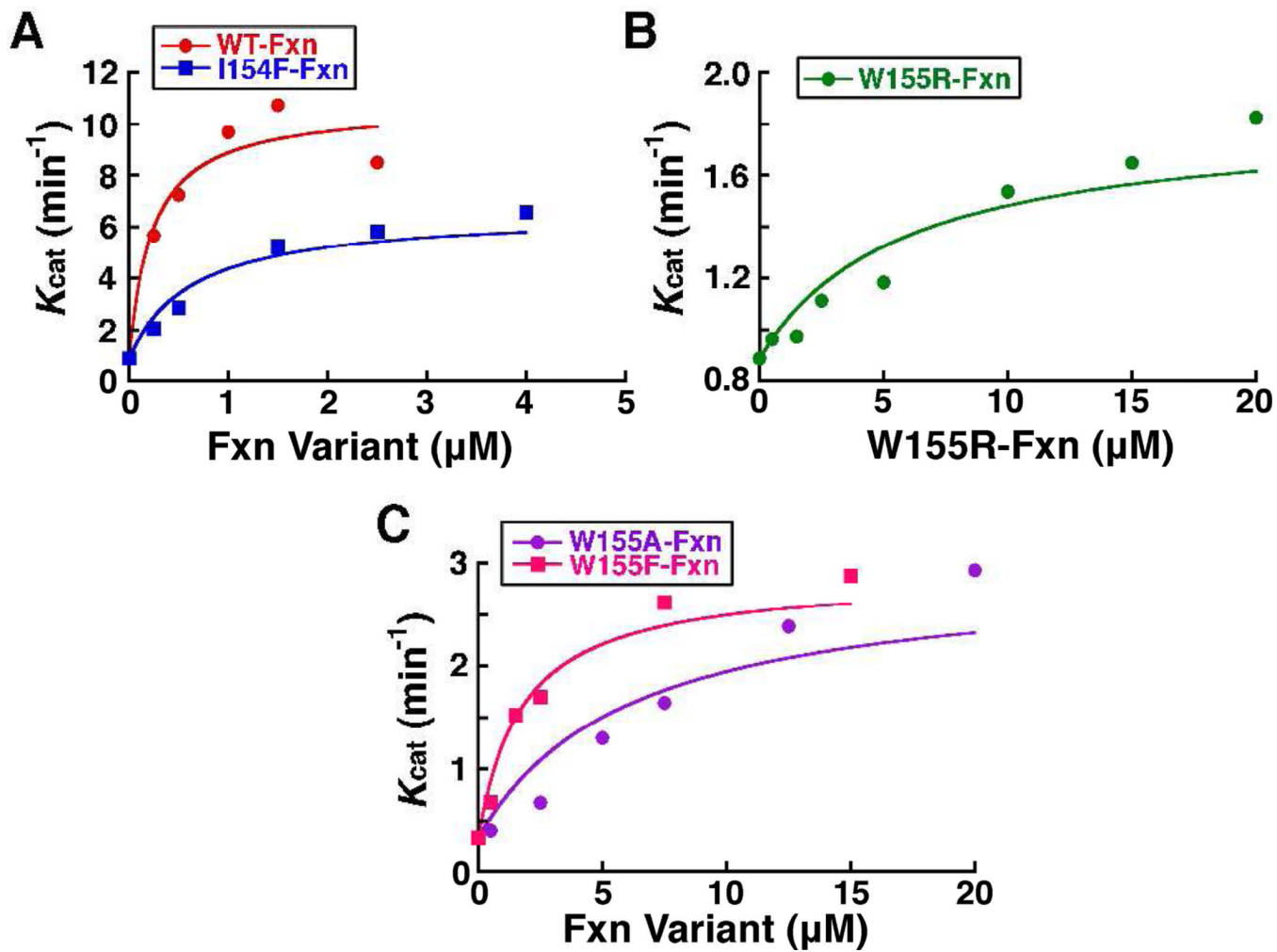
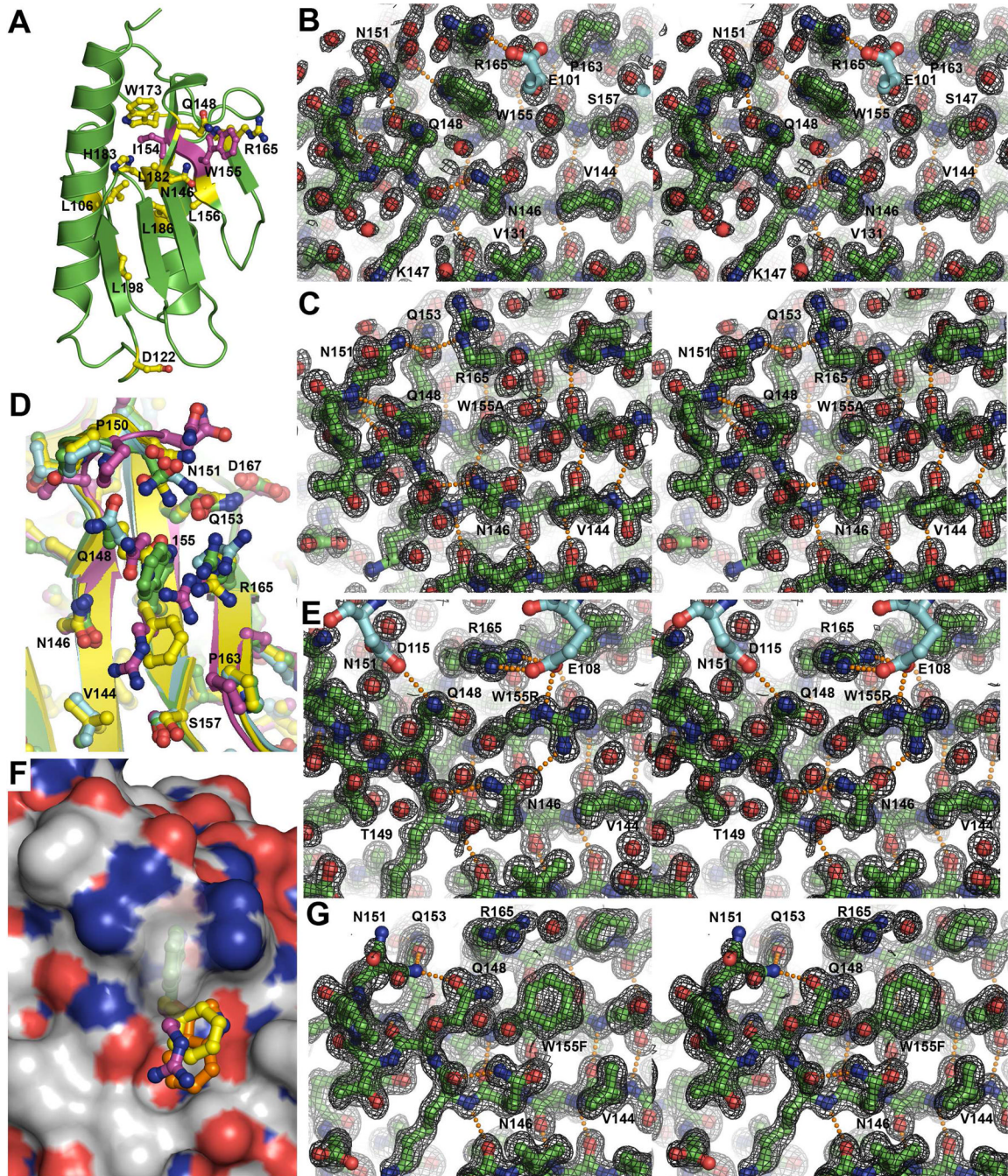


Figure 2.

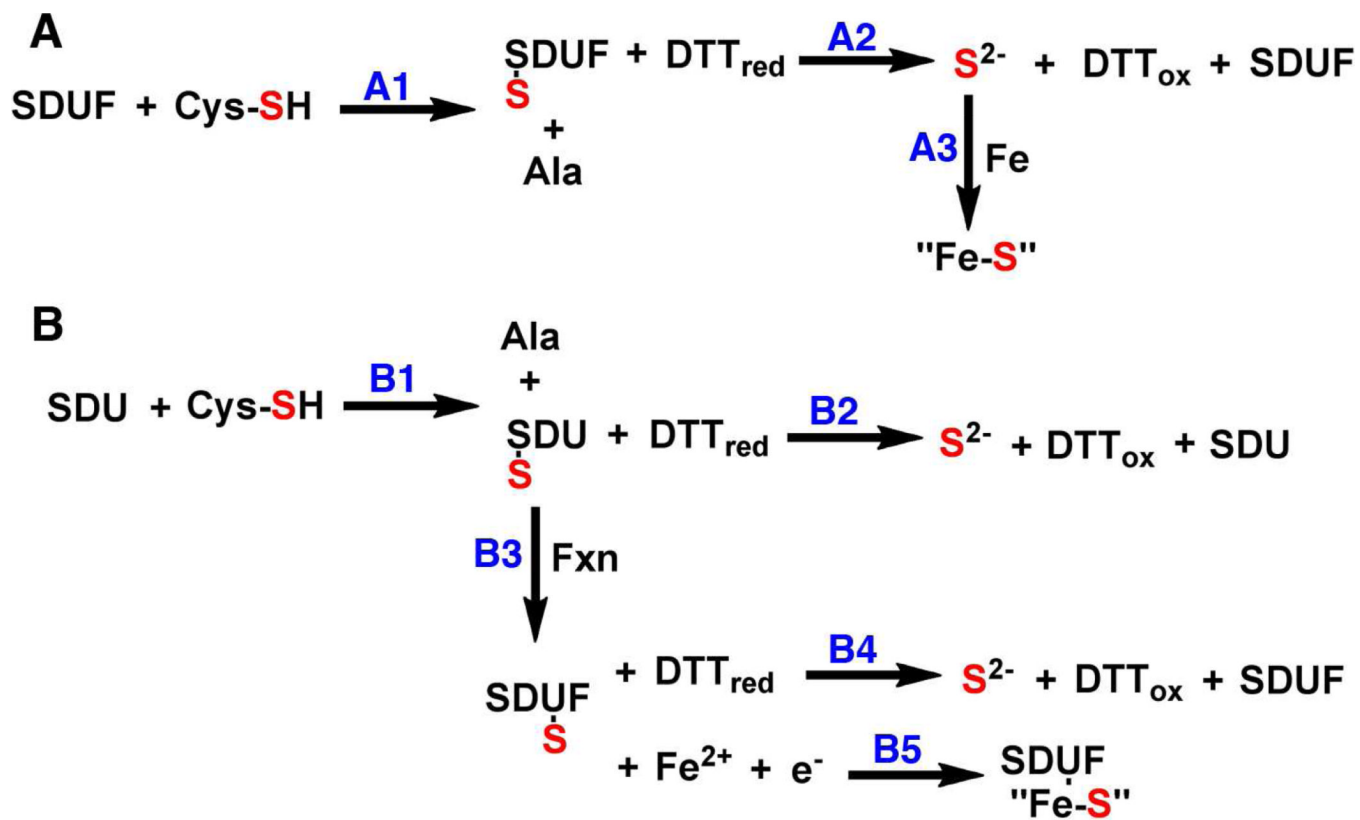
Fxn variants exhibit diminished Fe-S cluster assembly activity. Fe-S cluster formation was monitored by an increase in absorbance at 456 nm as a function of time. Assays included Nfs1/Isd11 with 3 equivalents of Isu2 and 3 equivalents of Fxn variants. The lines through the data are the fits using first-order kinetics. Control samples without Fxn and with Na₂S rather than cysteine are included.

**Figure 3.**

Determination of binding constants for Fxn variants. The k_{cat} was determined at different Fxn concentrations. The lines through the data are the fits as a Type II allosteric activator to equation [1]. The R^2 values are 0.925, 0.947, 0.899, 0.882, and 0.964 for the Fxn, I154F, W155RW155A, and W155F variants, respectively.

**Figure 4.**

Crystallographic structures of Fxn and the W155A, W155R and W155F variants. A) FRDA missense mutations (yellow) mapped onto the structure of Fxn. The I154F and W155R mutants are shown in magenta. Stereo images with 2Fo-Fc electron density contoured at 1 sigma for (B) Fxn; (C) W155A; (E) W155R; and (G) W155F structures. Symmetry molecules are shown without electron density in cyan. Panel D displays an overlay of native Fxn (green), W155A (cyan), W155R (magenta), and W155F (yellow) structures. Panel F displays a molecular surface of native Fxn along with the side-chain for the W155R (magenta), W155F (yellow), and a modeled conformer of W155 (orange). Residue W155 is shown with a semi-transparent molecular surface.

**Figure 5.**

Alternate schemes for *in vitro* sulfide production and Fe-S cluster assembly by the human assembly system. See text for details.

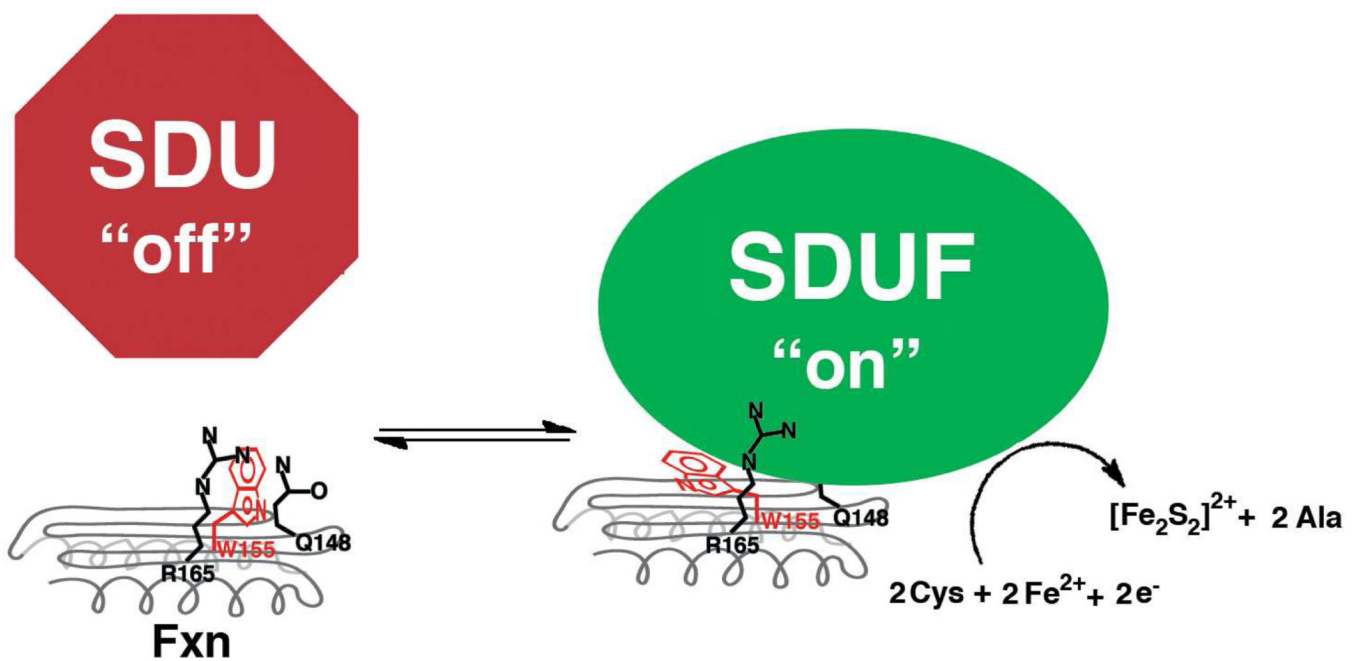


Figure 6.
Cartoon of induced-fit model for Fxn binding and activating the SDU complex.

Table 1

The Rate of Fe-S cluster formation and Binding and Rate Constants for Nfs1 Activity with Fxn Variants

Complex	Nfs1 activity (min ⁻¹)	Fe-S cluster formation (min ⁻¹)	Fxn K_d (μM)	k_{cat} (min ⁻¹)	$K_M^{Cys(mM)}$	k_{cat}/K_M (M ⁻¹ s ⁻¹)	Age of onset ¹	Fxn expression ¹
SDU + Fxn ²	8.25 ± 0.90	12.3 ± 0.4	0.22 ± 0.05	8.5 ± 0.3	0.014 ± 0.002	9800 ± 1700	NA	100
SDU + I154F	4.14 ± 0.20	7.6 ± 0.5	0.63 ± 0.14	6.6 ± 0.4	0.025 ± 0.004	4400 ± 800	16	18
SDU + W155R	0.60 ± 0.07	0.9 ± 0.1	6.73 ± 1.28	1.8 ± 0.1	0.013 ± 0.003	2300 ± 500	4	18
SDU + W155A	0.83 ± 0.28	2.0 ± 0.1	6.12 ± 1.36	3.9 ± 0.2	0.012 ± 0.003	5600 ± 1600	NA	NA
SDU + W155F	2.09 ± 0.51	3.4 ± 0.1	1.78 ± 0.31	4.5 ± 0.1	0.018 ± 0.003	4100 ± 800	NA	NA
SDU ²	0.65 ± 0.02	0.7 ± 0.1	NA	0.89 ± 0.04	0.59 ± 0.05	25 ± 3	NA	NA

¹ From reference (8).

² Kinetic data from reference (34).

Table 2

X-ray Data Collection and Refinement Statistics

Fxn Variants	WT	W155A	W155R	W155F
Data Collection				
Wavelength (Å)	0.97945	1.03315	0.97945	0.97945
Space Group	P2 ₁ 2 ₁ 2 ₁	C2	P2 ₁ 2 ₁ 2 ₁	P2 ₁
Unit cell (Å and °)	42.9, 44.8, 69.0 90°, 90°, 90°	87.5, 32.3, 44.8 90°, 91.4°, 90°	38.9, 49.2, 67.1 90°, 90°, 90°	47.7, 53.1, 48.5 90°, 112.3°, 90°
Resolution (Å)	44.86-1.30	44.797-1.50	39.68-1.31	34.27-1.50
Outer shell (Å)	1.37-1.30	1.58-1.50	1.38-1.31	1.58-1.50
Observations	258690	147672	476216	237470
Unique Observations	33576	20101	31647	35399
Redundancy	7.7	7.3	15.0	6.7
Completeness (%) [*]	100.0 (100.0)	99.3 (98.6)	99.8 (99.7)	97.7 (97.2)
Mean I/(σI) [*]	14 (2.6)	12.0 (6.6)	22.2 (5.6)	13.8 (2.2)
R _{sym} (%) ^{*†}	8.2 (62.4)	13.8 (48.3)	6.4 (41.3)	7.2 (88.4)
Refinement				
Residues not in model	82-88, 210	82-89	82-87, 209-210	82-84, 210
Solvent atoms	201	101	169	138
Ligand		SO ₄	Mg	Mg
R _{work} /R _{free} (%) [‡]	15.3/18.7	16.9/19.2	15.1/19.7	16.4/21.3
r.m.s.d. bond lengths (Å)	0.032	0.029	0.023	0.023
r.m.s.d. bond angles (°)	2.7	2.6	1.8	1.9
Average B-factor (Å²)				
Protein	16.8	9.9	13.2	22.2
Water	60	34.6	60	40
Ramachandran (%)				
Most favored	93.4	91.5	93.4	94.8
Additional allowed	6.6	8.5	6.6	5.2
Generous	0	0	0	0
Disallowed	0	0	0	0
PDB code	3S4M	3S5D	3S5E	3S5F

^{*} Values in parentheses are the statistics for the highest resolution shell of data

[†] R_{sym} = S | I_{hkl} - <I> | / S <I>, where <I> is the average individual measurement of I_{hkl}.

[‡] R_{work} = (S |F_{obs} - F_{calc}|) / S|F_{obs}|, where F_{obs} and F_{calc} are the observed and calculated structure factors, respectively. R_{free} is calculated the same as R_{work}, but from the data (5%) that were excluded from the refinement.